

Roughening and melting of Au(110) surfaces

A. Hoss and M. Nold

Institut für Nukleare Festkörperphysik, Kernforschungszentrum Karlsruhe, P.O. Box 3640, W-7500 Karlsruhe 1, Germany

P. von Blanckenhagen

*Institut für Materialforschung, Kernforschungszentrum Karlsruhe,
P.O. Box 3640, W-7500 Karlsruhe 1, Germany*

O. Meyer

Institut für Nukleare Festkörperphysik, Kernforschungszentrum Karlsruhe, P.O. Box 3640, W-7500 Karlsruhe 1, Germany

(Received 1 May 1991; revised manuscript received 3 December 1991)

The structure of the Au(110) surface was investigated in the temperature range between 60 and 1250 K by the ion channeling and blocking method using an electrostatic energy analyzer. An anomalous temperature dependence of the blocking pattern was found around 680 K which may be caused by a roughening transition. Above 770 K the number of visible atom layers increases faster with increasing temperature, as expected from the temperature dependence of the mean vibration amplitude. The number of observed disordered (110) layers follows a logarithmic growth law as predicted by the premelting theory and molecular dynamics simulations.

I. INTRODUCTION

As shown by recent experiments¹⁻⁷ as well as by molecular dynamics calculations and simulations,⁸⁻¹¹ some open metal surfaces, Pb(110) or Al(110) surfaces for instance, begin to melt far below their bulk melting point T_M . For fcc crystals it was found experimentally that surface melting is present on (110) and absent on (111) and (100) surfaces.

At around 70% of T_M a distinct increase of the number of visible (110) layers is observable, assuming that the experimental technique allows a precise measurement of the quasiliquid-layer thickness. Out of several surface-sensitive methods, medium-energy ion spectroscopy (MEIS) was shown to be the most suitable technique for the direct measurement of the number of disordered layers, provided that the energy resolution of the spectrometer is high enough to obtain nearly layer by layer resolution.

MEIS was applied in the study of the melting behavior of Pb(110) (Refs. 2-6) and Al(110).¹ It could be shown that the temperature dependence of the number of disordered layers can well be understood within the framework of the Landau-Ginzburg theory of surface melting.^{12,13} One expects a temperature-dependent divergence of the number of layers, which are visible to the ion beam and detector, in comparison to the increase due to the mean vibration amplitude of the surface atoms. The difference between the measured number of layers and the expected number of layers for the given temperature or vibration amplitude is a direct measure of the thickness of the quasiliquid layer.

This thickness was shown to follow first the logarithmic law $\sim \ln[T_0/(T_M - T)]$, where T_0 is a characteristic material-dependent temperature (see Sec. III). For temperatures very close to the bulk melting point

($T_M - 0.5$ K) the dependence is expected to be a power law $\sim (T_M - T)^{-1/3}$.

In this paper a temperature-dependent study of the structure of the Au(110) surface is presented in the temperature range from 60 K to 1250 K, which is 90 K below the bulk melting point at $T_M = 1337$ K. Au(110) shows at low temperatures¹⁴ a (2×1) *missing-row* reconstruction. The order-disorder transition of the (2×1) reconstruction appears at a critical temperature T_c of (670 ± 20) K.^{15,16} For temperatures around T_c a roughening transition is predicted.¹⁷⁻¹⁹

Only a few experiments with x-ray diffraction,²⁰ low energy ion scattering,²¹ and low-energy electron diffraction (LEED) (Ref. 22) have investigated step densities at the Au(110) surface. It was shown that the roughening transition will generate a high step density at the Au(110) surface, which disappears for higher temperatures.²² By low energy ion scattering²¹ it was shown that a threshold for the formation of atomic steps lies around T_c .

Beside these experimental data for the Au(110) surface structure molecular dynamics simulations¹⁰ predict that above the $(2 \times 1) \rightarrow (1 \times 1)$ deconstruction transition a liquidlike surface disorder appears near 70% of T_M . The thickness of the quasiliquid layer grows logarithmically as expected for a system governed by short-range forces.²³ This premelting effect for the open Au(110) surface is expected also by considering thermodynamical calculations.²

The purpose of our investigation of the Au(110) surface was to check these predictions by the MEIS technique and to prove whether or not surface roughening with a following premelting of the surface occurs. Indications of surface roughening and evidence for premelting of the Au(110) surface were found by analyzing the energy spectra and position distributions of the backscattered ions,

which were measured by the ion channeling and blocking method using an electrostatic energy analyzer equipped with a position sensitive detector.

The experimental data and details of sample preparation are described in Sec. II. The results of our measurements are given in Sec. III and discussed in Sec. IV by considering the results in terms of the present theoretical models for the surface melting effect.

II. EXPERIMENTAL

A. Setup of the MEIS experiment

MEIS connected with a high-resolution energy spectrometer equipped with a toroidal electrostatic energy analyzer (TEA), has been used previously²⁻⁶ with great success to detect and investigate surface melting on Pb(110) and Al(110) surfaces. The detailed description of the apparatus and method is given in Refs. 24-26. In our experiments a 300-keV proton (${}^1_1\text{H}^+$) or alternatively helium (${}^4_2\text{He}^+$) beam was used. The obtained data for the for the different ion beams can be compared by rescaling the He-beam data about the difference between a Monte Carlo simulation for the He and H beam. The beam is produced by a Van de Graaf accelerator. The experiments were performed with an ion current of $I_{\text{beam}} = 0.4 \mu\text{A}$ measured on the sample and an energy stability of the accelerator better than 100 eV.

The crystal was positioned in a double alignment geometry where the incident beam is aligned with the $\langle \bar{1}01 \rangle$ and the mean axis of the TEA with the $\langle 011 \rangle$ direction with an accuracy better than 0.05° . As the alignment of the sample relative to the ion beam and detector is along low-indexed crystal directions, the top-most atoms of the crystal cause a shadow cone on the inward path of the impinging ions and block the ions on their outward trajectory. These effects make the method surface sensitive so that the position signal of the backscattered ions shows a distinct minimum on the outward detection direction which is called a *blocking dip*. On the other hand, the energy spectrum shows a surface peak (SP) because the scattering intensity from the bulk atoms is strongly suppressed by the shadowing effect. By analyzing the area of the surface peak (SPA) and calibrating this SPA to the yield obtained at random incidence of the ion beam to the crystal a direct value for the number of surface atoms per unit area^{1,24} is measurable. These random orientations of the crystal were produced by rotating the sample to positions of the space vector (Θ, Φ, α) which were chosen by a computer random-number generator.

Disordered layers, whose atoms are displaced from lattice sites, will give an additional contribution to the SPA of an ideal, well-ordered crystal. This can be understood because those layers do not participate in the shadowing-blocking effect. The area density of disordered layers can be determined by subtracting the number of layers obtained from a Monte Carlo simulation of the ordered surface²⁷ from the measured number of visible layers. The measured and simulated number of visible atoms per unit area are averaged over the blocking dip full width at half maximum (FWHM). The simulation regards the

experimental parameters as lattice structure, relaxation, beam parameters, and mean vibration amplitudes of bulk and surface atoms at given temperatures.²⁸

The experiments were performed in an UHV chamber with a pressure of 4×10^{-8} Pa. The UHV surface melting study can be regarded to take place in equilibrium with Au vapor since the evaporation rate of Au atoms is very small due to the Au vapor pressure of 8×10^{-8} Pa at 1000 K. To check the crystalline quality of the surfaces the chamber is equipped with a LEED system.

B. Surface preparation

The surface of the Au crystal (10 mm diameter, 3 mm thick) was oriented with an accuracy of $10-15'$ parallel to the (110) plane. A platinum wire (0.5 mm diameter) which fits into a slot on the side of the crystal fixed the crystal on the Mo sample holder. The sample holder is placed on a three-axis goniometer and is equipped with a resistance heater and a Ni-Cr-Ni thermocouple for temperature measurement. The temperature was stabilized with a programmable PID controller within 0.1 K. Cryogenic temperatures were reached by cooling the sample with a copper braid, which is connected to a continuous-flow helium cryostat.

The (110) crystal was cleaned by Ar^+ -ion sputtering with 0.5-2 keV for 20-30-min duration with an emission current of 30 mA, 450 K and an incidence angle of 45° and subsequent annealing at 750 K for several hours (2-10). To obtain a homogenous sputtering the sample was rotated under the Ar^+ -ion beam. We checked another Au crystal of the same quality and with the same cleaning procedure in a different UHV chamber by Auger electron spectroscopy. After the above-mentioned sputtering procedure the contamination was less than the detection limit of 1% of a monolayer. To check contaminations on the Au surface directly in the UHV chamber a MEIS impurity investigation was done before each experiment. This was done by measuring the total energy spectrum of backscattered particles up to the Au-SP energy at $k^2 E_0$, where k^2 is the kinematic factor of the elastic collision and E_0 the incident energy (300 keV). The detection limit for C and O was found to be 8% of a monolayer.

To achieve the complete (2×1) *missing-row* reconstruction the surface had to be annealed once again at 520 K after sputtering for 2 min with 0.5-keV Ar^+ ions.²² The surface structure was finally checked by LEED. The (2×1) pattern showed sharp spots on our reverse view LEED optics, thus indicating a well-ordered surface structure. After this procedure the crystal was turned into the described *double alignment* geometry $\langle \bar{1}01 \rangle \rightarrow \langle 011 \rangle$.

III. RESULTS

The experiments were performed with a 300-keV proton beam and the geometry described above. The beam geometry is depicted in Fig. 1 which shows the missing-row reconstruction, relaxation, and the buckling of the third layer caused by the missing atom rows on the top layer.

The number of visible (110) monolayers, which con-

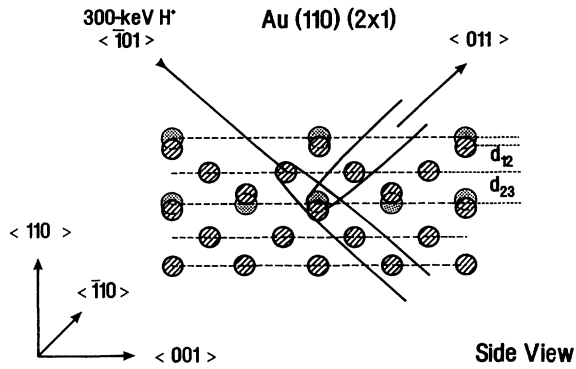


FIG. 1. Scattering geometry: The Au(110) (2×1) surface in double alignment geometry, the impinging particles are protons of 300 keV energy. The dotted circles show the positions of a perfect crystal. The striped circles show the situation for the real crystal with relaxation and buckling

tribute to the surface peak (SP), can be obtained by integrating the backscattered yield over the SP and calibrating this quantity as described in Sec. II. In this analysis a minimum number of monolayers is expected in the $\langle 011 \rangle$ blocking direction at $\theta = \theta_{\text{block}}$. The shape of the blocking pattern obtained from SP integration is characteristic for the vibrational behavior of the atoms which contribute to the SP for the following reasons.

Regarding the increase of the mean vibration amplitude with temperature it can be understood that atoms of deeper layers become more and more visible. This is due to the fact that the location probability outside the shadow cone increases for these atoms. So the total number of visible layers will increase with temperature.

But the width of the blocking dip taken at half maximum also shows a characteristic temperature behavior. The probability that the backscattered particles will not undergo a perfect blocking process increases with a higher vibration amplitude of the surface atoms and so the backscattered intensity increases due to the additional scattering processes for angles around θ_{block} reducing the total blocking dip width. One expects a continuously decreasing FWHM of the blocking dip with temperature. Some typical blocking patterns which show the described behavior are displayed in Fig. 2 for different temperatures.

We measured the blocking dip in the temperature range from 300 K to 1240 K and observed a deviation from the expected temperature dependence as derived by the Monte Carlo simulation (Fig. 3). A fit to the measured blocking profiles of Fig. 2 shows a minimum of the FWHM at 680 K. The fit function was an inverse Gaussian distribution overlayed to a first-order polynomial. The FWHM values were taken from the Gaussian distribution.

Figure 4 shows the surface peaks for some typical temperatures between 470 K and 1240 K. For temperatures $T > 770$ K the surface peak area (SPA) increases much faster. Each peak is well separable in the studied temperature range. The background was subtracted from the

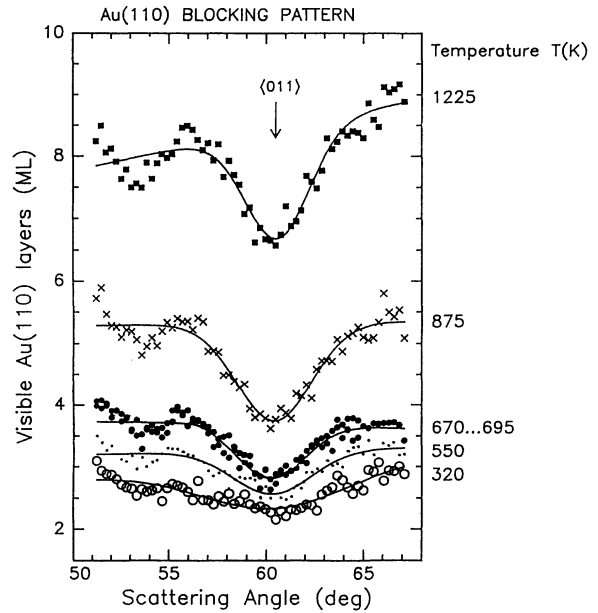


FIG. 2. Au(110) blocking pattern at various temperatures showing the decrease of the $\langle 011 \rangle$ blocking dip FWHM with temperature. Each point represents the integrated backscattering intensity under the surface peak calibrated against random height; the solid line is a Gaussian fit to the data (see also text).

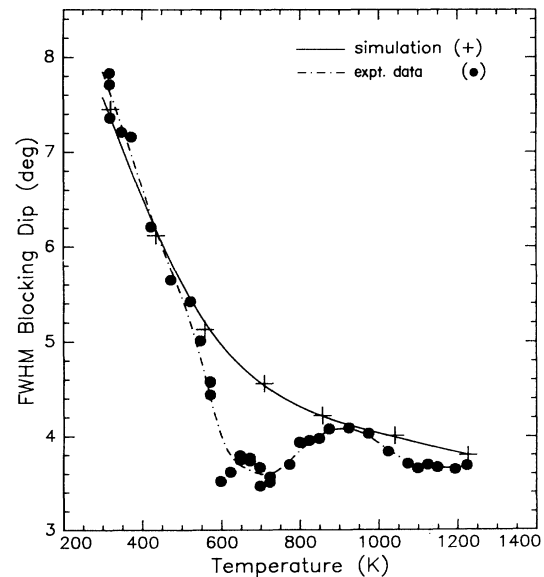


FIG. 3. FWHM of the Au(110) $\langle 011 \rangle$ blocking dip as function of temperature. The dot-dashed line is a fit to the measured FWHM values. The solid line is a fit to the blocking dip width obtained by the Monte Carlo simulation for an ordered surface.

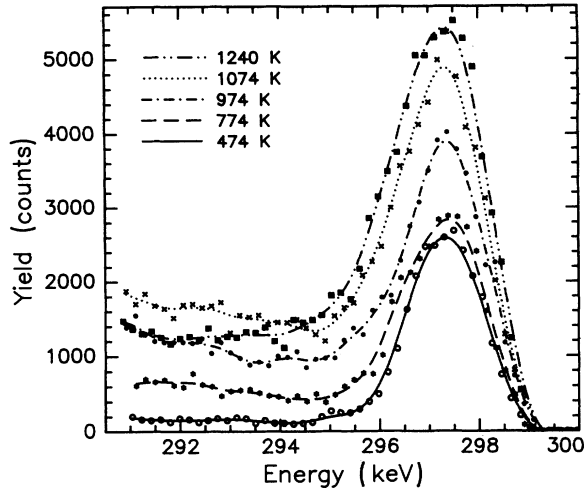


FIG. 4. Surface peaks as function of temperature: The energy spectra at some different temperatures show the broadening and increase of the surface peak at $k^2 E_0$, with E_0 the incident energy of the protons (300 keV) and k^2 the kinematic collision factor.

SPA linearly by correction about the area under the line between the minimum yield counts behind the SP and the mean energy of the peak. We can exclude the possibility that the observed effect is due to damage of the surface by the ion beam. The χ_{\min} value behind the SP would then show a nonproportional increase with temperature. The MEIS data were also taken at different spots on the sample.

The conversion of the surface peak area into the number of visible Au(110) monolayers [one monolayer (1 ML) corresponds to a single (110) atomic plane which is equivalent to 8.49×10^{14} atoms cm^{-2}] in the temperature range from 60 K to $(T_M - 90)$ K shows a temperature dependence which is plotted in Fig. 5. The result of the Monte Carlo simulation²⁷ is drawn as a solid line.

The simulation regards following crystal parameters. First- and second-layer relaxations were chosen to be $\Delta d_{12}/d = -18\%$ and $\Delta d_{23}/d = +4\%$, respectively. Buckling of the third layer was also considered with a 14% shift from the lattice sites (0.2 \AA).²⁸ The relaxation values are kept constant for temperatures above T_c . The vibration is assumed to be isotropic and uncorrelated and is simulated by a three-dimensional Gaussian distribution. Since the vibration amplitudes of the first ($L1$) and second layer ($L2$) are greater than the bulk value they were chosen to be $\sigma_{L1} = 1.5\sigma_{\text{bulk}}$ and $\sigma_{L2} = 1.3\sigma_{\text{bulk}}$ for $T < T_c$. For temperatures above the deconstruction transition temperature these amplitudes are expected to be greater. This was regarded by the simulation by $\sigma_{L1} = 2.0\sigma_{\text{bulk}}$ and $\sigma_{L2} = 1.5\sigma_{\text{bulk}}$. The temperature-dependent values for the vibration amplitudes were calculated from the Debye temperature for Au $\Theta_D = 170$ K. A typical bulk value at 700 K is $\sigma_{\text{bulk}} = 0.13 \text{ \AA}$. The simulation results in a linear increasing number of visible layers due to the increase of the vibration amplitude of

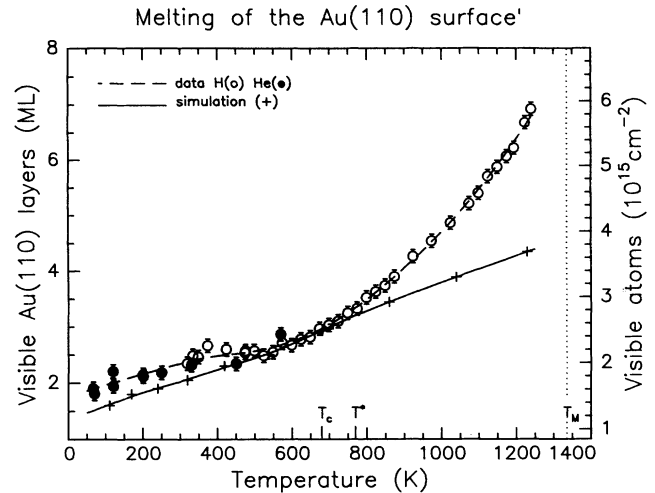


FIG. 5. Au(110) surface peak area as function of temperature: The number of disordered layers increases starting at 770 K due to surface melting. The solid line represents the Monte Carlo simulation (Ref. 27) for a -18% relaxed top layer and $+4\%$ (Ref. 28) relaxed second layer. The vibration amplitudes of the first and second layers were increased for $T > T_c$ compared to the values for $T < T_c$. The dashed line is a spline fit to the experimental data. The filled circles represent results with helium ions as impinging particle. These points were normalized by comparison to proton simulation data.

the atoms contributing to the surface peak with temperature. The slope of the increase is greater for $T > T_c$.

For temperatures below 400 K the experimental data were also obtained by a He beam (filled circles). To compare these data with the H-beam data they were rescaled as mentioned above. The experimental results exceed the simulated results about 0.5 ML. We assume that this could be due to a higher vibration amplitude or a lattice distortion, which would make more monolayers visible to the ion beam and detector. The observed plateau between 450 K and 650 K indicates an influence of the order-disorder transition to the number of visible (110) layers. Near T_c the vibrational motions of the outermost atoms are assumed to be more correlated. This would result in a decrease of the visible atoms per unit area.

Above 770 K the experimental data increase much faster than the simulated results. T^* is the temperature above which the creation of disorder on the surface begins. We conclude that this increase of number of visible Au(110) monolayers is due to a creation of a thin quasiliquid layer. The data are reversible and reproducible.

To check the growth law of the quasiliquid layer, which is assumed to be a logarithmic law, the number of disordered layers, calculated as the difference between experimental and simulated data, is plotted versus a logarithmic $(T_M - T)$ temperature scale. Figure 6 shows that the data can well be parameterized by a logarithmic growth law. Fitting the data yields the following experimental law for the growth of the quasiliquid layer thickness for temperatures greater than $T^* = 770$ K:

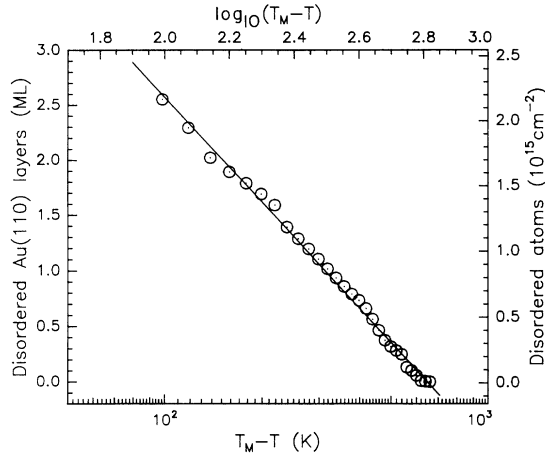


FIG. 6. Disordered layer thickness: Number of disordered monolayers on the Au(110) surface plotted vs an inverse logarithmic temperature scale up to 90 K below the bulk melting point T_M showing that the data fit well to the theoretical exponential growth law.

$$N_{\text{eq}}(T) = 1.16 \times 10^{15} \ln \left(\frac{639.7}{T_M - T} \right) \quad (\text{atoms cm}^{-2}). \quad (1)$$

$N_{\text{eq}}(T)$ is the number of disordered atoms per cm^{-2} at thermal equilibrium. Equation (1) agrees well with the predicted growth law for surface melting.²

IV. DISCUSSION

How can we explain the minimum of the blocking dip width at 680 K? One possible explanation for this anomaly may be an increase of the vibration amplitudes in this temperature range. An increase of the mean vibration amplitude can be expected for a surface above the roughening temperature. The edge atoms partici-

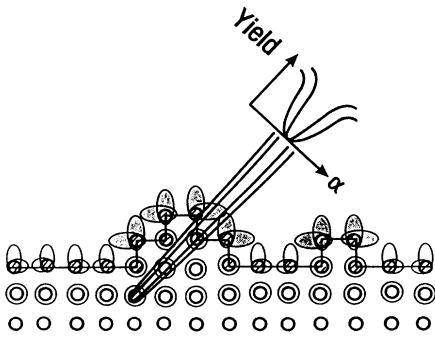


FIG. 7. Schematic illustration of MEIS on a rough surface: The anisotropic vibration amplitudes of the atoms located in a surface step are shown by dotted ellipses. The increased amplitudes of the two top-layer atoms are illustrated by circles of larger diameter.

pating in a step of a rough surface are assumed to have a larger and more anisotropic vibration amplitude compared to atoms of a smooth surface. To illustrate this behavior the amplitudes of the edge atoms in a surface step are drawn in Fig. 7 as dotted ellipses. The increased amplitudes of the one- and two-layer atoms are shown by larger circles. Additional scattering processes on the surface will occur in blocking direction and result in a decrease of the dip width.

But this is only one explanation for the observed anomaly. For a straightforward analysis we have to ex-

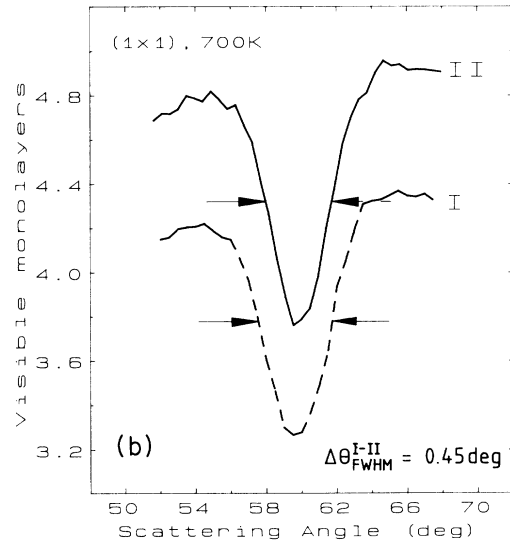
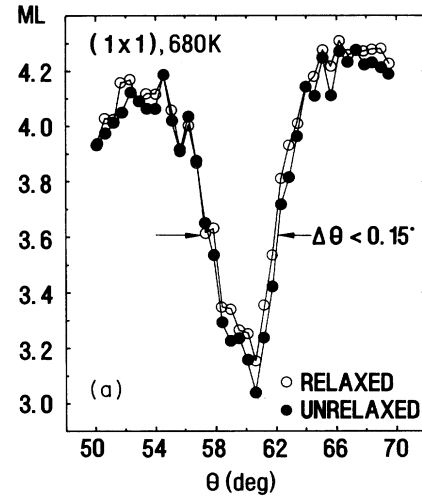


FIG. 8. Simulation results concerning influences on the blocking dip shape: (a) Strong relaxation change of the top layer at 680 K for the (1×1) phase. The relaxation of the first interlayer distance changes from $\Delta d_{12}/d = -18\%$ (o) to an unrelaxed surface (\bullet). (b) Enhancement of an anisotropic vibrational amplitude of first- and second-layer atoms at 700 K for the flat surface in the (1×1) phase. The different blocking profiles I and II are discussed in the text.

clude other effects. Possibly a strong relaxation change might occur at the top layer. This possibility was checked by another simulation for the (1×1) phase at 680 K. A strong change of the top-layer relaxation ($\Delta d_{12}/d = -18\%$) to an unrelaxed top layer gave no significant change in the width of the blocking dip. The difference of the FWHM was less than 0.15° , which is in the order of the position-sensitive detector resolution (0.1°). Two typical blocking curves for the relaxed and unrelaxed Au(110) surface are shown in Fig. 8(a). But the difference between simulated and measured FWHM of the blocking dip as depicted in Fig. 3 is about 0.9° at 680 K thus indicating that the relaxation change cannot explain the anomaly.

The influence of an anisotropic and strongly increased vibrational amplitude on the width of the blocking dip was also simulated for a flat surface. Figure 8(b) shows the result of such a simulation with two blocking profiles at 700 K. The three orthogonal components of the vibrational amplitudes $(\sigma_x, \sigma_y, \sigma_z) = \sigma$ of first ($L1$) and second layer ($L2$) were simulated by three Gaussian distributions with the z direction parallel to the surface normal. The components for curve I were $\sigma_{L1}^I = (2.2, 2.2, 1.5)\sigma_{\text{bulk}}$ and $\sigma_{L2}^I = (1.5, 1.5, 1.5)\sigma_{\text{bulk}}$. For curve II the components of the vibrational amplitude vectors were increased to $\sigma_{L1}^{II} = (5.0, 5.0, 3.0)\sigma_{\text{bulk}}$ and $\sigma_{L2}^{II} = (2.5, 2.5, 2.5)\sigma_{\text{bulk}}$. This increase and anisotropy of the vibrational amplitude results in a decrease of the blocking dip width about $\Delta\Theta = 0.45^\circ$. However, the increase and anisotropy on a rough surface might be even stronger.

Because MEIS is a method which is sensitive to the mean area density of the surface structure, the observed decrease up to 680 K may be understood as an increase of the step density at the Au(110) surface. As mentioned above the simulation takes into account the $(2 \times 1) \rightarrow (1 \times 1)$ deconstruction transition by a change of the vibration amplitudes of the two top layers. Therefore we would not expect that the minimum is due to the deconstruction transition. Another reason for this is that for temperatures greater than 680 K the FWHM approaches the simulated curve again, thus indicating a decrease of the surface step density. The observed minimum of the width of the blocking dip may be related to the vacancy and step formation, recently observed by LEIS.²¹

Also a LEED study²² had shown that the step density decreases above 720 K due to a smoothing of the rough surface. We conclude that the observed anomaly may be explained by a roughening transition where the step atoms vibrate anisotropically with an enhanced amplitude compared to the bulk atoms.

The growth law of the observed quasiliquid-layer thick-

ness can be derived from a Landau-Ginzburg-type theory of surface melting. van der Veen, Pluis, and van der Gon²³ showed that short-range interactions between the surface atoms result in a logarithmic temperature dependence of the disordered layer thickness.

For temperatures very close to the bulk melting point [$< (T_M - 0.3 \text{ K})$] a departure from the logarithmic law into a power law with exponent $(-1/3)$ is predicted. Experimental indications have been found only for the Pb(110) surface.⁶ This departure can also be understood with the above theory, where it was shown that long-range interactions will be more important at temperatures near T_M compared to short-range interactions between the surface atoms. For the Au(110) surface we could not check this prediction, but we could confirm the logarithmic growth law:

$$N_{\text{eq}}(T) = N_0 \ln \left(\frac{T_M \Delta\gamma}{(T_M - T)L_M N_0} \right) \text{ (atoms cm}^{-2}\text{)}. \quad (2)$$

N_0 is a material specific constant of microscopic dimensions ($\sim 10^{15} \text{ atoms cm}^{-2}$) and L_M the latent specific heat for melting per Au atom ($8.35 \times 10^{-20} \text{ J}$). The quantity $\Delta\gamma$ represents the free-energy balance per unit surface area, about which it is energetically favorable for a dry surface to be completely wetted by a liquid layer. Pluis, Frenken, and van der Veen² showed with a simple thermodynamic model that surface melting will only occur when this energy balance is positive. The free-energy balance is defined by subtracting the specific free energies γ_{lv} and γ_{sl} from γ_{sv} at the bulk melting temperature T_M for the interfaces liquid-vapor, solid-liquid, and solid-vapor. The microscopic constant N_0 follows the relation

$$N_0 = \left(\frac{\rho_l \xi_l}{2} \right). \quad (3)$$

ρ_l is the density of the liquid disordered Au layer ($5.9 \times 10^{22} \text{ atoms cm}^{-3}$) and ξ_l the correlation length of the short-range interactions. The physical meaning of ξ_l is that it represents the distance after which the surface order parameter has changed about a factor e . We calculated a value of $3.9 \pm 0.2 \text{ \AA}$ for ξ_l . $(T_M \Delta\gamma)/(L_M N_0)$ in Eq. (2) has the dimension of temperature ($= T_0$). From our fit to the experimental data we obtained 639.7 K which gives for the energy balance $\Delta\gamma$ of the interfaces per unit surface area a value of $(46.6 \pm 0.8) \times 10^{-3} \text{ J/m}^2$. From the literature values,²⁹ which are quite uncertain (especially γ_{sl} and γ_{lv} are not accurately known at T_M) one extracts an expected energy balance of $\Delta\gamma = 33 \times 10^{-3} \text{ J/m}^2$.

It should be pointed out that our experimental values for the characteristic quantities of surface melting agree

TABLE I. Overview about characteristic premelting quantities.

Surface	Ref.	Method	ξ_l (\AA)	$\Delta\gamma$ (10^{-3} J/m^2)	T_0 (K)	T^* (K)
Pb(110)	3	MEIS	6.2	21.2	55	≈ 450
Al(110)	1	MEIS	4.9	29.2	117.67	≈ 750
Au(110)	10	molecular dynamics simulation	4.4 ± 0.6	49.4	630 ± 350	< 1000
Au(110)	this study	MEIS	3.9 ± 0.2	46.6	639.7	770

well not only with the theory, but also with molecular dynamics simulations of the Au(110) surface performed by Ercolessi *et al.*¹⁰

These simulations with $20 \times 40 \times 32$ atoms and periodic boundary conditions predict a correlation length $\xi_l = 4.4 \pm 0.6 \text{ \AA}$ and a $\Delta\gamma$ of $49.4 \times 10^{-3} \text{ J/m}^2$.

So far only open fcc (110) surfaces, for which $\Delta\gamma > 0$, showed the surface melting effect.¹⁻⁶ To summarize our results for the Au(110) surface in comparison to the other MEIS studies of the metal surfaces Pb(110) and Al(110), which were shown to premelt,^{1,3} Table I gives an overview about the characteristic quantities for premelting.

We conclude that by this study evidence for the premelting effect of the Au(110) surface is given. The experimental MEIS results confirm nicely the results of the

molecular dynamics simulation.¹⁰ But it must still be checked whether a power law near the bulk melting point occurs and whether the closer packed Au surfaces do not show premelting because of their negative $\Delta\gamma$ value.

ACKNOWLEDGMENTS

The author is indebted to the FOM Instituut voor Atoom-en Molecuulfysica in Amsterdam, especially to J.F. van der Veen, J. Frenken, and W. Slijkerman for helpful discussions during the build up of our MEIS system in the Kernforschungszentrum Karlsruhe-INFP, and also for allowing us to use their Monte Carlo simulation package called VEGAS.

¹A.W.D. van der Gon, R.J. Smith, J.M. Gay, D.J. O'Connor, and J.F. van der Veen, *Surf. Sci.* **227**, 143 (1990).

²B. Pluis, J.W.M. Frenken, and J.F. van der Veen, *Phys. Rev. Lett.* **59**, 2678 (1987).

³J.W.M. Frenken and J.F. van der Veen, *Phys. Rev. Lett.* **54**, 134 (1985).

⁴J.W.M. Frenken, P.M. Marée, and J.F. van der Veen, *Phys. Rev. B* **34**, 7506 (1986).

⁵B. Pluis, J.W.M. Frenken, and J.F. van der Veen, *Phys. Scr.* **T19**, 382 (1987).

⁶B. Pluis, T.N. Taylor, D. Frenkel, and J.F. van der Veen, *Phys. Rev. B* **40**, 1353 (1989).

⁷P. von Blanckenhagen, W. Schommers, and V. Voegelé, *J. Vac. Sci. Technol. A* **5**, 649 (1987).

⁸P. Stoltze, J.K. Nørskov, and U. Landman, *Phys. Rev. Lett.* **61**, 440 (1988) [Al(110)].

⁹E.T. Chen, R.N. Barnett, and U. Landman, *Phys. Rev. B* **41**, 439 (1990) [Ni(110)].

¹⁰F. Ercolessi, S. Iarlori, O. Tomagnini, E. Tosatti, and X.J. Chen, *Surf. Sci.* **251/252**, 645 (1991).

¹¹P. Carnevali, F. Ercolessi, and E. Tosatti, *Phys. Rev. B* **36**, 6701 (1987).

¹²R. Lipowsky and W. Speth, *Phys. Rev. B* **28**, 3983 (1983).

¹³R. Lipowsky, *Ferroelectrics* **73**, 69 (1987).

¹⁴W. Moritz and D. Wolf, *Surf. Sci.* **88**, L29 (1979).

¹⁵D.E. Clark, W.N. Unertl, and P.H. Kleban, *Phys. Rev. B* **34**, 4379 (1986).

¹⁶J.C. Campuzano, M.S. Forster, G. Jennings, and R.F. Willis, *Phys. Rev. Lett.* **54**, 2684 (1985).

¹⁷J. Villain and L. Vilfan, *Surf. Sci.* **190**, 4379 (1986).

¹⁸M. den Nijs, *Phys. Rev. Lett.* **64**, 435 (1990).

¹⁹A.C. Levi and M. Tonzani, *Surf. Sci.* **218**, 223 (1989).

²⁰I.K. Robinson, Y. Kuk, and L.C. Feldman, *Phys. Rev. B* **29**, 4762 (1984).

²¹E. van de Riet, H. Derks, and W. Heiland, *Surf. Sci.* **234**, 53 (1990), and references therein.

²²U. Romahn, H. Zimmermann, M. Nold, A. Hoss, H. Göbel, P.v. Blanckenhagen, and W. Schommers, *Surf. Sci.* **241/242**, 656 (1991).

²³J.F. van der Veen, B. Pluis, and A.W.D. van der Gon, in *Kinetics of Ordering and Growth at Surfaces*, edited M.G. Lagally (Plenum, New York, 1990), and references therein.

²⁴J.F. van der Veen, *Surf. Sci. Rep.* **5**, 199 (1985), and references therein.

²⁵W.C. Turkenburg, W. Soszka, F.W. Saris, H.H. Kersten, and B.G. Colenbrander, *Nucl. Instrum. Methods* **132**, 587 (1976).

²⁶R.G. Smeenk, R.M. Tromp, H.H. Kersten, A.J.H. Boerboom, and F.W. Saris, *Nucl. Instrum. Methods* **195**, 581 (1982).

²⁷J.W.M. Frenken, R.M. Tromp, and J.F. van der Veen, *Nucl. Instrum. Methods B* **17**, 334 (1986), and references therein.

²⁸M. Copel and T. Gustafsson, *Phys. Rev. Lett.* **57**, 723 (1986).

²⁹A.R. Miedema, F.J.A. den Broeder, and R. Boom, *Z. Metallk.* **69**, 183 (1978); **69**, 287 (1978); **70**, 14 (1979).

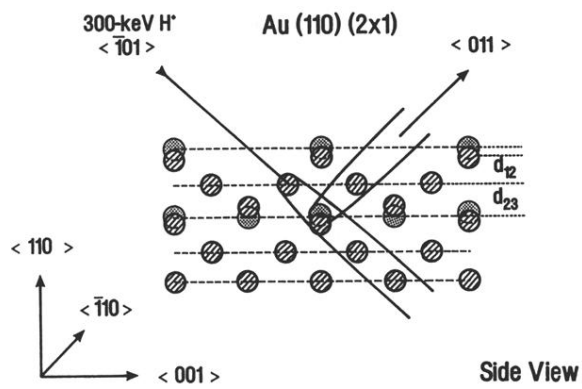


FIG. 1. Scattering geometry: The Au(110) (2x1) surface in double alignment geometry, the impinging particles are protons of 300 keV energy. The dotted circles show the positions of a perfect crystal. The striped circles show the situation for the real crystal with relaxation and buckling

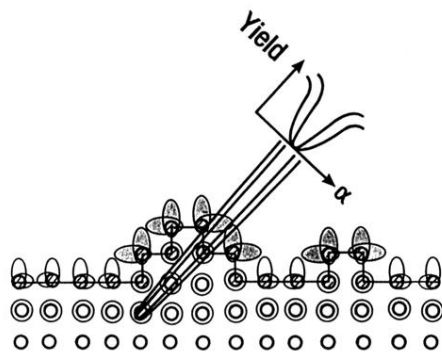


FIG. 7. Schematic illustration of MEIS on a rough surface: The anisotropic vibration amplitudes of the atoms located in a surface step are shown by dotted ellipses. The increased amplitudes of the two top-layer atoms are illustrated by circles of larger diameter.